ORIGINAL ARTICLE

Multi-functional vesicles improve *Helicobacter pylori* eradication by a comprehensive strategy based on complex pathological microenvironment

Xiaonan Chen[a], Yiqing Zou[a], Shuqi Zhang[a], Pengchao Fang[a], Shuxuan Li[a], Pengyu Li[a], Yingying Sun[a], Gang Yuan[b,c], Haiyan Hu[a,d,*]

[a]*Lab of Pharmaceutics, School of Pharmaceutical Sciences, Sun Yat-sen University, Guangzhou 510006, China*
[b]*Phase I Clinical Trial Center, the First Affiliated Hospital of Sun Yat-sen University, Guangzhou 510080, China*
[c]*Department of Geriatrics, the First Affiliated Hospital of Sun Yat-sen University, Guangzhou 510080, China*
[d]*Guangdong Provincial Key Laboratory of Chiral Molecule and Drug Discovery, Sun Yat-sen University, Guangzhou 510006, China*

Abstract *Helicobacter pylori* (*H. pylori*), creating a global infection rate over 50%, presents great challenges in clinical therapies due to its complex pathological microenvironment *in vivo*. To improve the eradication efficacy, herein we fabricated a pharmaceutical vesicle RHL/Cl-Ch-cal where cholesterol-PEG, calcitriol and first-line antibiotic clarithromycin were co-loaded in the rhamnolipid-composed outer lipid layer. RHL/Cl-Ch-cal could quickly penetrate through gastric mucus layer to reach *H. pylori* infection sites, and then effectively destroyed the architecture of *H. pylori* biofilms, killed dispersed *H. pylori* and inhibited the re-adhesion of residual bacteria (called biofilms eradication tetralogy). Moreover, RHL/Cl-Ch-cal activated the host immune response to *H. pylori* by replenishing cholesterol to repair lipid raft on the cell membrane of host epithelial cells. Finally, RHL/Cl-Ch-cal killed the intracellular *H. pylori* through recovering the lysosomal acidification and assisting degradation. In experiments, RHL/Cl-Ch-cal demonstrated prominent anti-*H. pylori* efficacy in the classical *H. pylori*-infected mice model. Therefore, the study provides a "comprehensive attack" strategy for anti-*H. pylori* therapies including biofilms eradication tetralogy, immune activation and intracellular bacteria killing.

*Corresponding author.
E-mail address: lsshhy@mail.sysu.edu.cn (Haiyan Hu).

1. Introduction

Helicobacter pylori (*H. pylori*) colonizing digestive tracts infects more than 50% of population worldwide[1]. Up to date, quadruple therapy is applied as the most effective choice in overcoming *H. pylori* antibiotics resistance. However, antibiotics resistances steadily increase causing the therapy failure rates to keep climbing[2]. *H. pylori* may directly damage gastric epithelial cells through virulence factors and lead to many related gastric diseases[3], while the population attributable risk percentage (PARP) of *H. pylori* was high up to 23.66% according to the epidemiological effect estimation for gastric cancer[4]. Moreover, *H. pylori* infection has a detrimental impact on the efficacy of cancer immunotherapies[5]. Therefore, improving the original treatment program or developing new therapies to eradicate *H. pylori* is urgently needed.

Among numerous factors, biofilms have been recently recognized as a main cause of antibiotics resistance as well as low eradication rate[6]. Endoscopically directed biopsies and scanning electron microscopy confirmed the presence of high-density *H. pylori* biofilms on the gastrointestinal mucosal surface of *H. pylori* positive patients[7,8]. Dense extracellular polymeric substances (EPS) protect *H. pylori* in biofilms, resulting in its antibiotics resistance 10−1000 times higher than that of planktonic ones[9,10]. After biofilms collapse triggered by stress, the dispersed *H. pylori* could re-adhere on the biotic surface to develop into new biofilms. Such an interconversion between planktonic bacteria and biofilms would eventually lead to persistent infections. Aiming at this interconversion, our previously established rhamnolipid (RHL)-composed nanoparticles based on "biofilms eradication tetralogy" could eradicate *H. pylori* biofilms effectively[11,12].

Even though overwhelming majority of *H. pylori* could be cleared after biofilms eradication, there was still a small portion of *H. pylori* left. Normally the residual bacteria can be identified and cleared by host immunity whereas *H. pylori* may subtly evade the immune system[13]. In chronic infections, *H. pylori* can deplete cholesterol (Chol) in host cell membrane[14], which further destroys the structure of Chol-rich lipid raft, wherein cytokine receptor subunits [*e.g.*, interferon-gamma receptor (IFNGR) for IFNG] would be decomposed at the same time. Then the downstream immune response (*e.g.*, JAK/STAT pathway) is blocked, and macrophage phagocytosis to *H. pylori* is interrupted as expected[15]. Therefore, activating immune response and avoiding excessive inflammation[16] would be a valid pathway to eradicate *H. pylori*. With regard to this, herein supplementing Chol was designed to repair damaged lipid raft, reconstruct receptor structure and activate downstream immune pathway.

Indeed, death is not the sole destiny of *H. pylori* after macrophage phagocytosis[17]. Ideally, intracellular *H. pylori* would be fused with lysosomes, where *H. pylori* finally could be killed by acidic hydrolases[18]. During lysosomal acidification, H^+ is absorbed while Ca^{2+} is excreted by calcium channel mucolipin 3 (MCOLN3) to maintain charge balance and achieve acidification and maturation[19]. Nevertheless, *H. pylori* may induce Ca^{2+} accumulation in lysosomes by down-regulating MCOLN3, resulting in abnormal acidification and the inability of hydrolase,

thus *H. pylori* survives and even leaves host cells by exocytosis to trigger new infections under appropriate conditions[20]. In this case, calcitriol that has the functionality of up-regulating MCOLN3 channel and promoting Ca^{2+} outflow and H^+ influx in lysosomes can restore lysosomal acidification and degradation abilities[20]. Thus, the combination of calcitriol and clarithromycin (CLR) was proposed herein, of which CLR was a first-line antibiotic against *H. pylori* assisting in killing intracellular *H. pylori* due to its easiness to enter host cells[21].

Successful eradication of *H. pylori* is a significant global public health challenge nowadays[22]. However, there is hardly any research focusing on the whole process of *H. pylori* infection and the multiple recrudescence reasons and taking into a comprehensive consideration on eradication strategy. Herein multi-drugs-loaded vesicles RHL/Cl-Ch-cal containing simple formulation and procedure but multi-functions were established (Scheme 1A). RHL/Cl-Ch-cal eradicated *H. pylori* through biofilms eradication tetralogy, immune response activation and intracellular bacteria killing (Scheme 1B). In detail, RHL layer destroyed biofilms structure and exposed interior *H. pylori*, while CLR could kill dispersed *H. pylori*. At the same time, Chol-PEG released from collapsed vesicles repaired lipid raft and reconstructed IFNGR subunits to activate downstream immune response and macrophage phagocytosis. Finally, the combination of calcitriol and CLR promoted lysosomal degradation of intracellular *H. pylori* by recovering lysosomal acidification.

2. Materials and methods

2.1. Cell lines, bacterial strain and mice

MGC803 cells and RAW264.7 cells were cultured in Dulbecco's modified Eagle medium (DMEM, Gibco, CA, USA) supplemented with 10% (*v/v*) fetal bovine serum (FBS, PAN-Biotech GmbH, Aidenbach, Germany), penicillin (100 U/mL, HyClone, Logan, USA) and streptomycin (0.1 mg/mL, HyClone) at 37 °C with 5% CO_2. *H. pylori* Sydney strain 1 (*H. pylori*, SS1) kindly provided by Guangdong Province Traditional Medical Hospital was cultured on Columbia blood agar plate (HKM, Guangzhou, China) supplemented with FBS, and incubated at 37 °C under microaerobic conditions (5% O_2, 10% CO_2, and 85% N_2). Sprague−Dawley rats (SD rats, 6−7 weeks old, body weight 220 ± 20 g) and female specific pathogen free (SPF) C57BL/6 mice (5−6 weeks old, body weight 20 ± 5 g) purchased from Guangdong medical laboratory animal center were fed with SPF feed and sterile water.

2.2. Preparation and characterization of RHL/Cl-Ch-cal

RHL/Cl-Ch-cal was prepared by film dispersion method. Rhamnolipid (RHL, Huzhou Zijin Biotechnology Co., Ltd., Huzhou, China), CLR (Cl, Aladdin Co., Ltd., Shanghai, China), Chol-PEG 2000 (Ch, Yuanye Bio-Technology Co., Ltd., Shanghai, China), calcitriol (cal, Aladdin Co., Ltd.) and DSPE-PEG 2000 (AVT Pharmaceutical Tech Co., Ltd., Shanghai, China) were dissolved
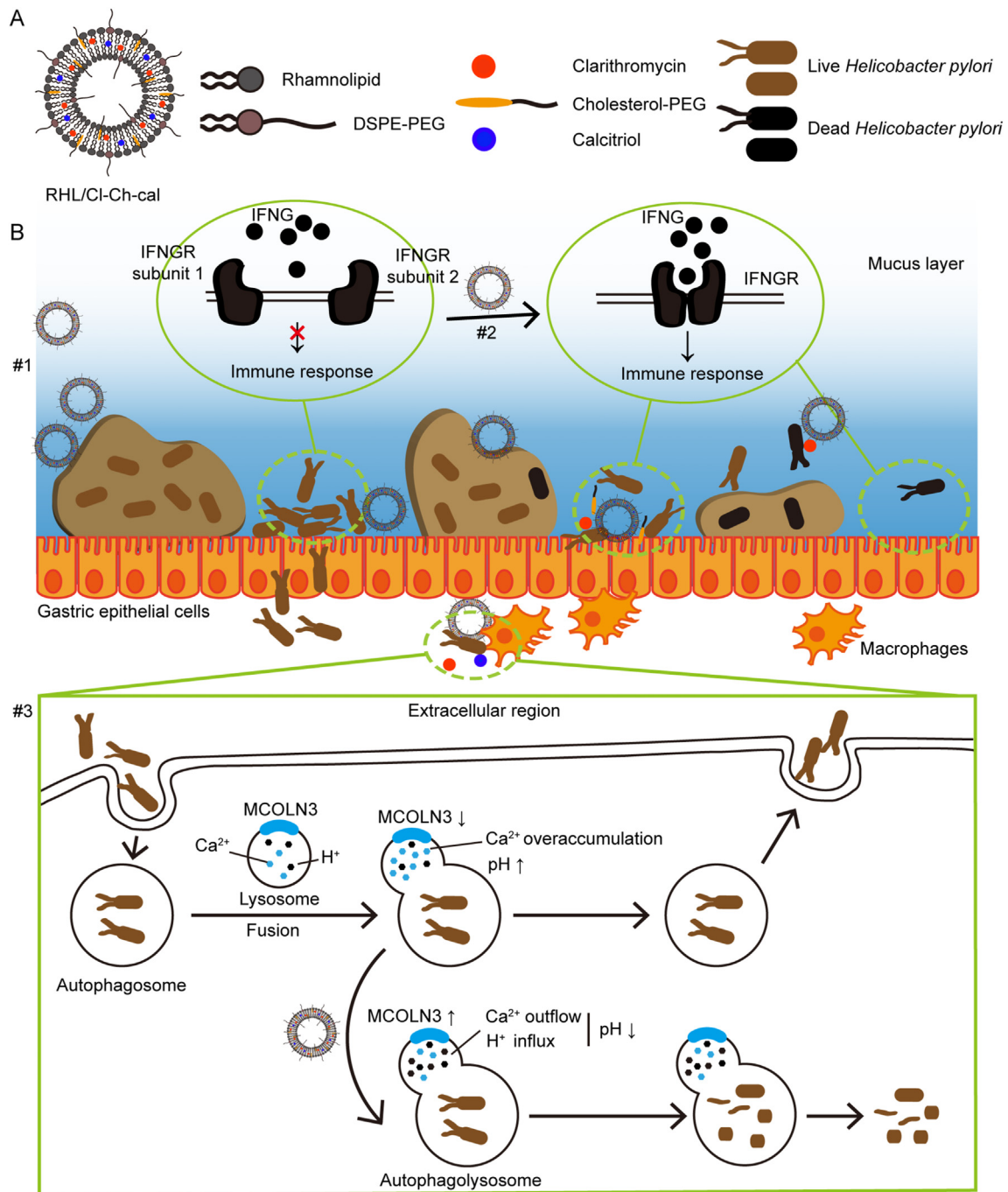
Scheme 1 Schematic diagram illustrating the composition and anti-*H. pylori* action of multifunctional RHL/Cl-Ch-cal. (A) The outer bilayer shell of RHL/Cl-Ch-cal was composed of RHL, where CLR (Cl), Chol-PEG (Ch) and calcitriol (cal) were loaded in the hydrophobic region. (B) RHL/Cl-Ch-cal comprehensively improved the *H. pylori* clearance rate by biofilms eradication tetralogy, immune activation and intracellular bacteria killing. #1 RHL/Cl-Ch-cal penetrated through gastric mucus layer, destroyed *H. pylori* biofilms to expose the interior *H. pylori* to CLR, which made *H. pylori* more easily to be killed, and then prevented bacteria from re-adhering to form new biofilms. #2 RHL/Cl-Ch-cal repaired the structure of lipid raft in epithelial cell membrane damaged by *H. pylori*, reconstructed the related cytokine receptors and recovered downstream immune responses. #3 RHL/Cl-Ch-cal assisted in regulating the balance of Ca^{2+} and H^+ in lysosomes and restored lysosomal acidification to degrade and kill intracellular *H. pylori*.

in chloroform at molar ratio of 156:1:125:6:22 and rotated to evaporate in flasks to form a film on the inner wall, and then sterile deionized water was added and stirred at 45 °C. To increase the stability and hydrophilicity of RHL/Cl-Ch-cal, Chol-PEG 2000

instead of Chol was used, and DSPE-PEG 2000 was added. For mucin binding assay and mucus penetration assay, RHL/Cl-Ch-cal was coated with chitosan (CS, 100−200 mpa.s, Aladdin Co., Ltd.), where RHL: CS = 1:2 (CS/RHL/Cl-Ch-cal). Besides, for

mucin binding assay and mucus penetration assay, coumarin 6 (Yuanye Bio-Technology Co., Ltd.) was loaded, while for the investigation of gastric retention, near-infrared fluorescent probe DiR (Yeasen, Shanghai, China) was loaded instead of CLR. Hydrodynamic diameter and zeta potential of RHL/Cl-Ch-cal were measured by ZetaSizer Nano ZS90 (Malvern Instrument, Nano ZS90, Malvern, UK), and morphological characteristics were observed by transmission electron microscopy (TEM, JEM1400, JOEL, Tokyo, Japan). For investigating the stability of RHL/Cl-Ch-cal in media, it was co-incubated with DMEM (with 10% FBS) and brain heart infusion broth (BHI, HKM) respectively, and then their particle sizes were measured at different time points. At the same time, RHL/Cl-Ch-cal was diluted to determine the particle size change. In addition, the stability of RHL/Cl-Ch-cal stored at 4 °C was measured. The drug encapsulation efficiencies were measured by high performance liquid chromatography (HPLC, Agilent Technologies Inc., Agilent 1260, CA, USA), in which RHL/Cl-Ch-cal were disintegrated by organic solvent after the unloaded drugs and RHL/Cl-Ch-cal were separated by centrifugal ultrafiltration at $5000 \times g$ for 10 min, and finally calculated according to Eq. (1):

$$\text{Encapsulation efficiency} (\%) = \frac{\text{Amount of encapsulated drug}}{\text{Total drug added}} \times 100 \tag{1}$$

2.3. In vitro drug release and leakage of RHL/Cl-Ch-cal

Free drugs and RHL/Cl-Ch-cal were placed in dialysis bags (MWCO of 2 kD, Viskase, IL, USA), respectively. The release media [pH 5.5, 1% (w/v) sodium dodecyl sulfate] were used for drug release study, while the release media [pH 2.0, 1% (w/v) sodium dodecyl sulfate] were used for drug leakage study. The dialysis bags were immersed into the release media at 37 °C with continuous shaking at 100 rpm. The media (1 mL) were collected at 0.25, 0.5, 1, 2, 6, 8, 12 and 24 h, respectively, and then the release media were replenished with the fresh media solutions (1 mL) at each time. The collecting solutions were analyzed by LC−MS/MS (Thermo, TSQ Quantum Access MAX, MA, USA) (for CLR) and HPLC (Agilent Technologies Inc.) (for calcitriol). The cumulative release rates and drug leakage percentage were calculated according to Eq. (2):

$$\text{Cumulative release/ drug leakage} (\%) = \frac{V_s \sum_{1}^{n-1} C_i + V_0 C_n}{m} \times 100 \tag{2}$$

where V_s was the volume of samples collecting each time, V_0 was the initial volume of the release media, C_i and C_n were the detected drug concentrations, i and n were the sampling times, and m was the total drug mass.

2.4. Mucin binding assay and mucus penetration assay

For mucin binding assay, coumarin 6-loaded RHL/Cl-Ch-cal and CS/RHL/Cl-Ch-cal were respectively mixed with 0.4% (w/v) mucin solution, and incubated at room temperature for 2 h. The supernatant was centrifuged and demulsified with organic solvent. Fluorescence intensity (excitation at 466 nm, emission at 500 nm)

was measured. According to Eq. (3), the amount of mucin aggregation was calculated.

$$\text{Mucin aggregation rate} (\%) = \frac{\text{FI}_0 - \text{FI}_1}{\text{FI}_0} \times 100 \tag{3}$$

where FI_0 was the fluorescence intensity of RHL/Cl-Ch-cal or CS/RHL/Cl-Ch-cal before incubation, FI_1 was the fluorescence intensity of RHL/Cl-Ch-cal or CS/RHL/Cl-Ch-cal in the supernatant after incubation.

For mucus penetration assay, fresh pig gastric mucus (40 mg) was added into donor Transwell chambers (3 μm pore size), sterile deionized water was placed in acceptor wells until it could contact the membrane of donor chambers. Coumarin 6-loaded RHL/Cl-Ch-cal and CS/RHL/Cl-Ch-cal were respectively added to the upper layer of mucus in donor chambers. After incubation at 37 °C, the solution in acceptor wells was collected and demulsified with organic solvent, finally fluorescence intensity was measured. The mucus penetration efficiency [apparent permeability coefficient (P_{app}) value] was calculated according to Eq. (4).

$$P_{app} = \frac{dQ}{dt \times A \times C} \tag{4}$$

where dQ/dt meant RHL/Cl-Ch-cal or CS/RHL/Cl-Ch-cal transport amount per unit time, A meant the membrane area of donor Transwell chambers, and C meant initial RHL/Cl-Ch-cal or CS/RHL/Cl-Ch-cal concentration.

2.5. Biofilm formation and crystal violet staining

H. pylori harvested from blood agar plates were adjusted to $\text{OD}_{600 \text{ nm}} = 0.2$ in BHI with 2% FBS. Then *H. pylori* suspensions were added into 48-well plates and incubated at 37 °C under microaerobic conditions for 72 h, followed by drugs incubation for 24 h. Crystal violet (CV) staining overall biomass consisted of bacteria and EPS was used to reflect the eradication effects of drugs. After removing planktonic bacteria, methanol was added to fix the remained biomass. Then, CV [1% (w/v)] stain lasted for 15 min, finally ethanol was added to dissolve CV and $\text{OD}_{570 \text{ nm}}$ was determined.

2.6. Measurement of EPS

After drugs treatment [free CLR, free CLR + amoxicillin (AMX, CLR: AMX = 1:2), RHL/Cl-Ch-cal], biofilm samples were collected by scrapers. Lyophilized EPS powders were obtained by ultrasonic fragmentation, high-speed centrifugation (11,000 rpm, 15 min), dialysis and freeze-drying. The contents of proteins and polysaccharides were respectively determined by bicinchoninic acid (BCA) protein assay kit (Thermo) and phenol-sulfuric acid method. Detailed methods were shown in our previous research[11]. In addition, FITC (50 μg/mL, excitation at 488 nm) and ConA-FITC (400 μg/mL, excitation at 488 nm) were used respectively to qualitatively label proteins and polysaccharides in biofilms, and then effect of drugs on EPS removal was observed through confocal laser scanning microscope (CLSM, Olympus Corporation, FV3000, Tokyo, Japan).

2.7.   Scanning electron microscope (SEM)

When culturing biofilms, *H. pylori* suspensions were inoculated in the well plates with cover glasses. After treated with drugs, biofilms were fixed in 2.5% glutaraldehyde for at least 3 h, and then 30%, 50%, 70%, 90% and 100% ethanol were used for gradient dehydration. Finally, the samples were dried by freeze-drying method, and the morphology of biofilms was observed by SEM (HITACHI, regulus 8230, Tokyo, Japan) after spraying gold.

2.8.   Minimal inhibitory concentration (MIC) assays

The gradient dilution drugs (free CLR, RHL/Cl-Ch-cal) were mixed with *H. pylori* suspensions and added to microplates, in which the concentration of final *H. pylori* was $OD_{600 \text{ nm}} = 0.1$. The microplates were placed at 37 °C under microaerobic conditions for 72−96 h with shaking (100 rpm). The MIC_{90} value was the minimum drug concentration that inhibited the growth of 90% *H. pylori*.

2.9.   Evaluation of inhibition of biofilm formation

H. pylori were collected into BHI containing 2% FBS and mixed with drugs, where the concentration of *H. pylori* suspension in the system reached $OD_{600 \text{ nm}} = 0.2$, and the concentration of CLR in each group was same (0.024 µg/mL, MIC), CLR: AMX = 1:2. The mixed solutions of *H. pylori* suspension and drugs were added into the microplates and incubated at 37 °C under microaerobic conditions for 4, 8, 12, 24 and 48 h respectively, and then stained by CV.

2.10.   Evaluation of biofilms survival

The *H. pylori* survival in biofilms was observed by CLSM (Olympus Corporation) after being labelled by LIVE/DEAD *Bac*Light Bacterial Viability kits (Invitrogen, CA, USA). After mature *H. pylori* biofilms were cultured, free CLR solutions of different concentrations (2.4, 4.8, 12 and 24 µg/mL) and RHL/Cl-Ch-cal containing different concentrations of CLR (1.2, 2.4, 4.8 and 24 µg/mL) were added for 24 h co-incubation, where the contents of other drugs were fixed in RHL/Cl-Ch-cal. Then biofilms were stained with a mixed dye of SYTO9 (1.67 µmol/L, labelling live and dead bacteria, excitation at 488 nm) and PI (10 µmol/L, labelling dead bacteria, excitation at 561 nm) for 15 min in the dark, followed by observation under CLSM.

2.11.   Activity of killing dispersed bacteria

The killing ability of RHL/Cl-Ch-cal against dispersed *H. pylori* from biofilms was detected through flat colony counting method. After drug incubation, the supernatants of biofilms samples in microplates wells were centrifuged at 8000 rpm for 3 min to remove drugs. BHI was used to resuspend *H. pylori* precipitates, which were spread on Columbia blood agar plates. The plates were cultured at 37 °C under microaerobic conditions for 72−96 h, and then the numbers of *H. pylori* colonies were examined.

2.12.   Macrophages migration assay

A two-cells co-culture model was established *in vitro* to investigate the effect of RHL/Cl-Ch-cal on enhancing the macrophages migration. MGC803 cells were first inoculated into the acceptor Transwell wells at 2.5×10^5 cells per well, and cultured at 37 °C (5% CO_2) for 24 h. *H. pylori* was infected with MGC803 cells in acceptor wells with a multiplicity of infection (MOI) of 1:10 for 24 h. After infection, RHL/Cl-Ch-cal were added into acceptor wells and RAW264.7 cells were inoculated into the donor Transwell chambers (8 µm pore size) at 10^5 cells per chamber at the same time, which was incubated at 37 °C (5% CO_2) for 4 h. Then, the media in donor chambers were removed, and methanol was added to fixed. After staining with 0.1% (*w*/*v*) CV, unmigrated RAW264.7 cells in donor chambers were wiped off with cotton swabs. Finally, microscopic examination.

2.13.   Chol supplement analysis

MGC803 cells were treated with methyl-β-cyclodextrin (Mβ-CD, 5 mg/mL) to deplete Chol in cell membrane. After drug treatment (here Chol-PEG 2000-FITC was loaded instead of Chol-PEG 2000, excitation at 488 nm), a mixture of DAPI (15 µg/mL, excitation at 405 nm) and DiD (4 µg/mL, excitation at 640 nm) was incubated with cells in the dark. The excess dye was washed by phosphate buffered saline (PBS) and then observed by CLSM.

2.14.   Detection of cell membrane polarity

Cells after drug treatment were collected and resuspended with 10 µmol/L laurdan (Macklin, Shanghai, China) for 5 min. After PBS washing, excitation wavelength was fixed at 380 nm, and emission spectrums of samples were scanned by fluorescence spectrometer (HORIBA, Fluoromax-4, CA, USA). Front entrance slit and front exit slit were both 5.00 nm. Laurdan generalized polarization (GP) was calculated according to Eq. (5):

$$GP = \frac{I_{440} - I_{490}}{I_{440} + I_{490}} \tag{5}$$

2.15.   Western blot (WB)

After drugs treatment, cells were lysed to obtain total proteins, which were then quantified by BCA protein assay kit. Protein samples were boiled with loading buffer, loaded into SDS-PAGE gel, and transferred to PVDF membrane. Then, the membrane was incubated with primary antibody [(IFNGR, JAK1 pY1022, STAT1 pY701, abcam, Cambridge, UK), (MCOLN3, novus, MO, USA), (β-actin, Cell Signaling Technology, Boston, USA)] overnight at 4 °C, and with secondary antibody [goat anti-rabbit IgG H&L (HRP), abcam] for 1 h. Finally, ECL luminescence developed. Semi-quantitative protein content was done by Image J (National Institutes of Health, MD, USA).

2.16.   Enzyme-linked immunosorbent assay (ELISA)

The cytokines were detected by quantitative sandwich enzyme-linked immunosorbent technique. After drugs treatments in MGC803 cells, samples were obtained after removing particulates by centrifugation at $1000 \times g$ for 15 min (2 °C−8 °C). Specific antibodies against human interleukin-8 (IL-8, MultiSciences, Hangzhou, China) and human β-defensins 3 (hBD-3, Cusabio, Wuhan, China) were pre-coated on plates respectively. Standard, samples, biotin-conjugated antibody and horseradish peroxidase (HRP)-labeled avidin were successively added in the plates. Color develops started through TMB substrate. Finally, absorbance was measured at 450 nm.

2.17. Evaluation of survival of intracellular bacteria

MGC803 cells and RAW264.7 cells were respectively infected with *H. pylori* at MOI 1:10 for 1 h. After infections, extracellular *H. pylori* was killed by gentamicin (200 μg/mL, Aladdin Co., Ltd.) for 2 h. Then, fresh media containing drugs with or without chloroquine (CQ, 20 μmol/L, Aladdin Co., Ltd.) were added for further cultivation for 24 h. At the end of incubation, 0.1% (*w/v*) saponin (Aladdin Co., Ltd.) was added to lyse cells, and cell lysates were collected and spread on Columbia blood agar plates to culture *H. pylori* at 37 °C under microaerobic conditions. *H. pylori* on the agar plates was collected and its turbidity was measured to determine the ability of killing intracellular *H. pylori*. For CLSM observation, carboxyfluorescein diacetate-succinimidyl ester (CFDA-SE, 2 μg/mL, Cayman, MI, USA) labelled *H. pylori*, DAPI (15 μg/mL, Yeasen) stained cell nuclei, and LysoTracker Red DND-99 (60 nmol/L, Yeasen) labelled lysosomes at the same time.

2.18. Determination of lysosomal acidity

After MGC803 cells and RAW264.7 cells had finished drugs treatment, LysoSensor Green DND-189 (1.2 μmol/L, Yeasen) was incubated at 37 °C with 5% CO_2 for 90 min. Excess dye was washed by PBS, cells were observed and photographed under CLSM (excitation at 488 nm). The mean fluorescence intensity of cells was calculated by Image J.

2.19. Measurement of lysosomal calcium level

After drugs treatments, MGC803 cells and RAW264.7 cells were washed by Hank's Balanced Salt Solution (HBSS) to remove the residual media. Then, cells were incubated with calcium fluorescent probe Fura-2 AM (1 μmol/L, Yeasen) at 37 °C for 30 min. After HBSS balancing for 20 min, Gly-Phe-β-naphthylamide (GPN, 70 μg/mL, APExBio, Houston, USA) was added to release calcium ions in lysosome. The fluorescence intensity was detected, where excitation wavelength was 340 nm and 380 nm, and emission wavelength was 510 nm. The concentration change of calcium ions in lysosome could be reflected by the ratio of fluorescence intensity (340 nm/380 nm).

2.20. Construction of H. pylori-infected mice model and pharmacodynamic evaluation

All the animal experiments were approved by the Institutional Animal Care and Use Committee of Sun Yat-sen University and conducted in conformity with the Guidelines for the Care and Use of Laboratory Animals. C57Bl/6 mice were randomly divided into two groups (blank group and model group). After fasting for 12 h, model group was given *H. pylori* suspension (1×10^8 CFU) every two days, and pregavage with 5% $NaHCO_3$ was to neutralize gastric acid. Repeated 7 times. Blank group only received PBS. Two weeks after *H. pylori* infection, ten randomly selected mice (5 mice in blank group and 5 mice in model group) were sacrificed, where whole gastric tissue was taken out and cut into homogenate, and then gastric DNA was extracted and quantitative real-time PCR (QPCR, Roche, lightCycler480II, Switzerland) was performed. *H. pylori* 16 S rDNA gene specific primers were as follow (F: 5′-CGCTAAGAGATCAGCCTATGTCC-3′; R: 5′-CCGTGTCTCAGTTCCAGTGTGT-3′). Rapid urease test was also used as a detection of *H. pylori* infection. Infected-mice were randomly divided into four groups (model, free CLR, triple therapy and RHL/Cl-Ch-cal). After continuous drugs administration for 5 days, all mice were sacrificed 3 days later. Stomach was divided into two parts, one of which was used to DNA extract, and then QPCR was performed to evaluate the clearance effect of *H. pylori* in C57Bl/6 mice. The other part was used for hematoxylin-eosin staining (H&E staining).

2.21. Investigation of gastric retention

Female C57Bl/6 mice were fasted for 12 h and divided into two groups. Gavage of free DiR (excitation at 748 nm, emission at 780 nm) and DiR-loaded RHL/DiR-Ch-cal (200 μL) were given into the stomachs of mice using No. 8 gavage needle. At the time points of 0, 1, 2, 4, 6, 8, 12 and 24 h, mice were sacrificed, and their stomachs were dissected and placed in the imaging system (Berthold, NightOWL II LB983, Bad Wildbad, Germany) for observation.

2.22. In-vivo pharmacokinetic study

SD rats were selected to study the pharmacokinetics of RHL/Cl-Ch-cal, where rats were randomly divided into 3 groups ($n = 3$). For the first group, rats were given a single dose of free CLR by intravenous injection. For the second and third group, rats were given a single dose of free CLR and RHL/Cl-Ch-cal by oral administration, respectively. During blood sampling, rats had full and free access to water all the time, and food was allowed 4 h after administration. After drug administration, venous blood (0.5 mL) was collected by retroorbital venous plexus puncture at the following time points and placed in heparin sodium pre-treated centrifuge tubes: 0.17, 0.33, 0.5, 0.75, 1, 2, 4, 6, 8, 10, 12 and 24 h. Then, plasma samples were obtained by centrifugation at 4000 rpm for 15 min, and stored at -20 °C till analysis. The plasma samples were treated by protein precipitation method (acetonitrile), where the ratio of plasma to acetonitrile was 1:3. After vortex for 3 min, the supernatant was obtained after centrifugation at 15,000 rpm for 10 min, and then analyzed by LC−MS/MS (Thermo).

2.23. Statistical data analysis

SPSS Statistics 22 (SPSS, IL, USA) was used to analyze the data. One-way ANOVA was used when the data satisfied homogeneity of variances and normal distribution. When the data did not meet these requirements, Welch's ANOVA was used for analysis. Differences with a P-value < 0.05 were considered significant.

3. Results and discussion

3.1. RHL/Cl-Ch-cal preparation and characterization

RHL/Cl-Ch-cal showed a classic structure of unilamellar spherical structure (Fig. 1A). Due to dehydration procedure during sample preparation for TEM observation, RHL/Cl-Ch-cal was observed with smaller particle size, while its hydration diameter was 137.5 ± 1.2 nm by dynamic light scattering (Fig. 1B). The encapsulation efficiency of RHL and Chol-PEG contents exceeded 80%, and that of CLR and calcitriol was over 70% in RHL/Cl-Ch-cal (Supporting Information Table S1).

To ensure the stability of RHL/Cl-Ch-cal in experiments *in vitro*, RHL/Cl-Ch-cal were co-incubated with DMEM (cell
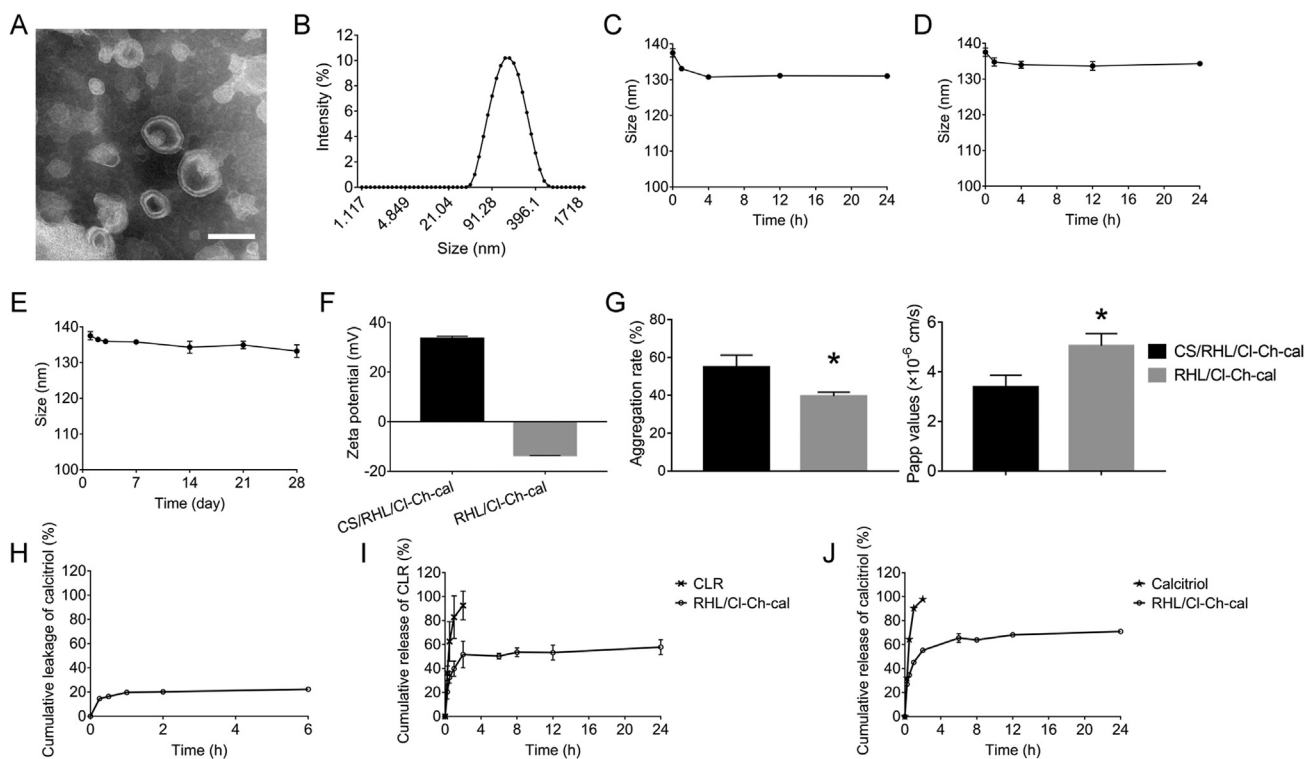
Figure 1 Characterization of RHL/Cl-Ch-cal ($n = 3$). (A) TEM image of RHL/Cl-Ch-cal. Scale bar = 100 nm. (B) Size distribution of RHL/Cl-Ch-cal by dynamic light scattering. The stability of RHL/Cl-Ch-cal in (C) DMEM, in (D) BHI and (E) during storage at 4 °C evaluated by the changes in particle size. (F) Zeta potential of RHL/Cl-Ch-cal and CS/RHL/Cl-Ch-cal. (G) Mucin aggregation rates and apparent permeability coefficients (P_{app}) of RHL/Cl-Ch-cal and CS/RHL/Cl-Ch-cal. *$P < 0.05$ *vs.* CS/RHL/Cl-Ch-cal. (H) Drug leakage of RHL/Cl-Ch-cal. (I) CLR release of RHL/Cl-Ch-cal. (J) Calcitriol release of RHL/Cl-Ch-cal.
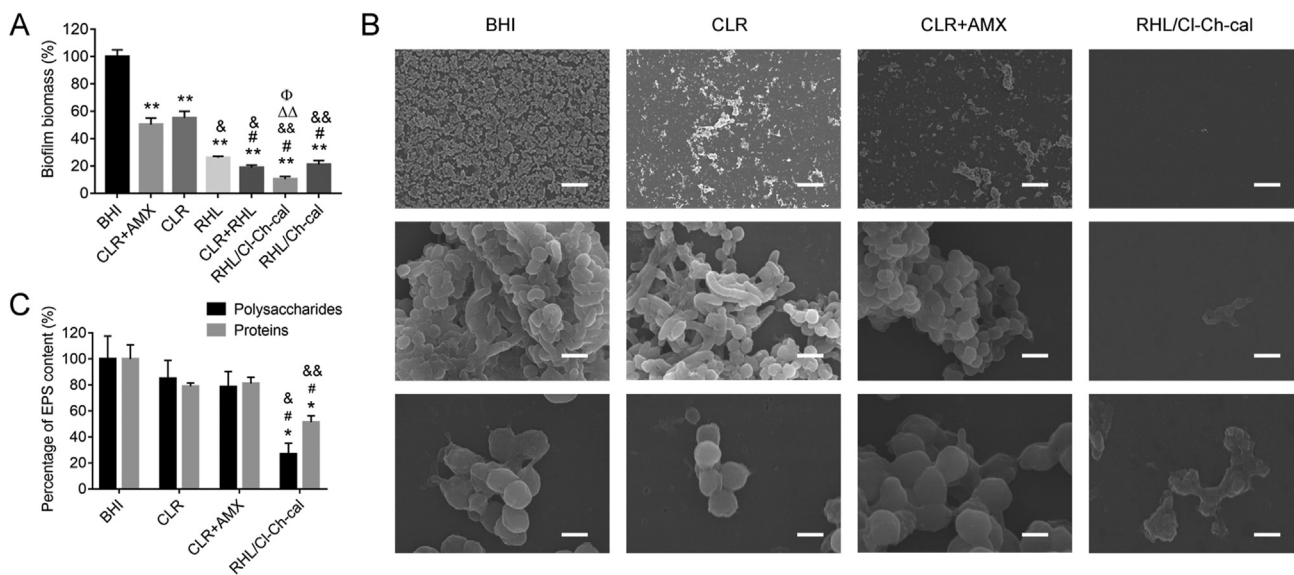

Figure 2 Biofilms eradication *in vitro*. (A) Biofilm biomass stained by CV after treatment with CLR + AMX, CLR, RHL, CLR + RHL, RHL/Cl-Ch-cal and RHL/Ch-cal ($n = 3$). **$P < 0.01$ *vs.* BHI, #$P < 0.05$ *vs.* CLR + AMX, &$P < 0.05$ and &&$P < 0.01$ *vs.* CLR, ΔΔ$P < 0.01$ *vs.* RHL, Φ$P < 0.05$ *vs.* CLR + RHL. (B) Residual biofilms by SEM observation. Scale bar = 30 μm in the top row, scale bar = 1 μm in the middle row, and scale bar = 450 nm in the bottom row. (C) The eradication of polysaccharides and proteins of EPS ($n = 3$). *$P < 0.05$ *vs.* BHI, #$P < 0.05$ *vs.* CLR, &$P < 0.05$ and &&$P < 0.01$ *vs.* CLR + AMX. The concentrations of CLR, AMX and RHL in the above preparations were 4.8, 9.6 and 600 μg/mL, respectively.
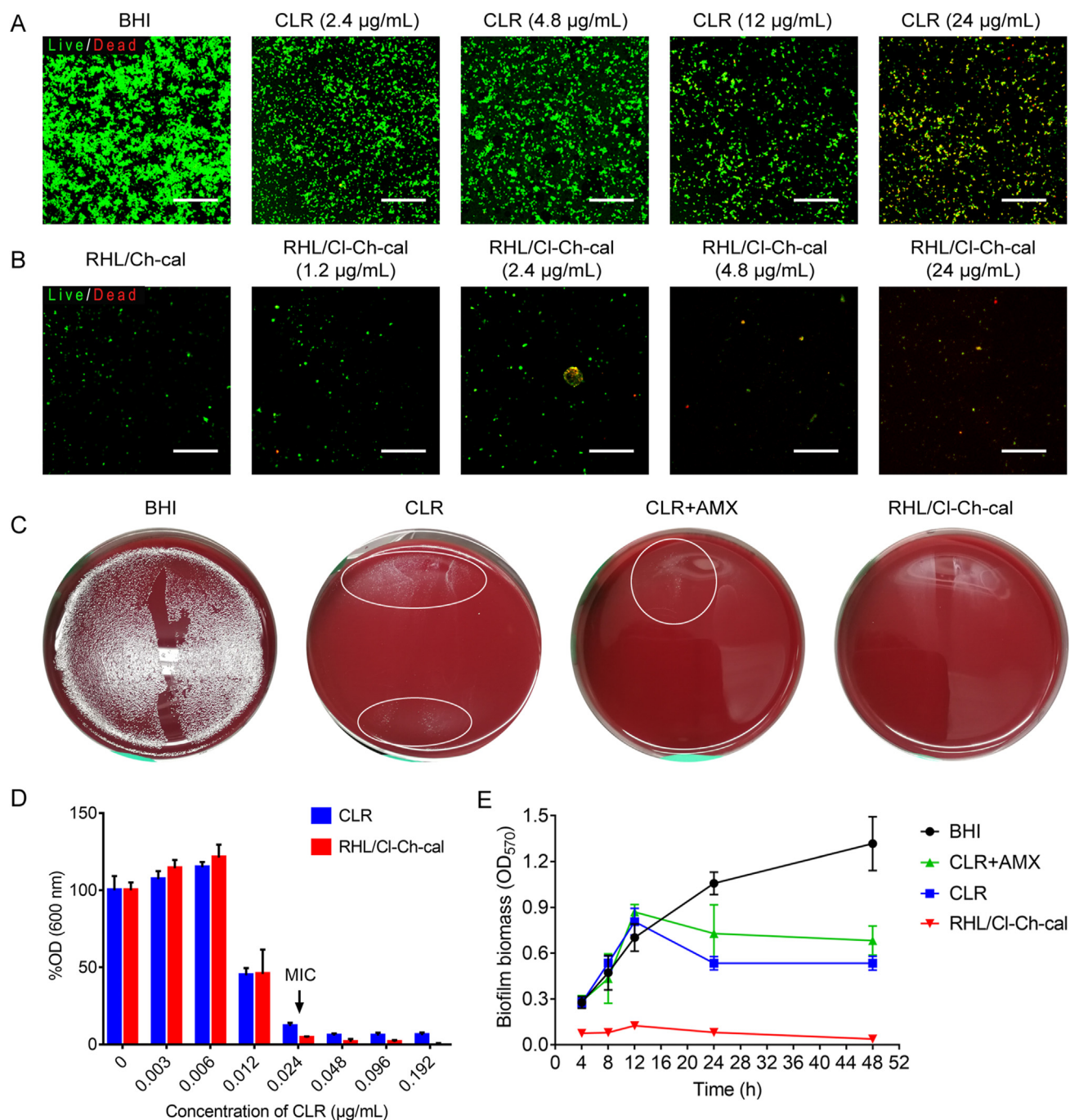
Figure 3 Killing bacteria and inhibiting the re-formation of *H. pylori* biofilms. The bacterial survival in *H. pylori* biofilms after treatments with different contents of (A) free CLR and (B) RHL/Cl-Ch-cal. Green fluorescence (SYTO 9) stained live and dead *H. pylori* while red fluorescence (PI) merely stained dead *H. pylori*; yellow represented PI and SYTO 9 overlay. Scale bar = 50 µm. (C) The culture of biofilm supernatants (including planktonic bacteria and bacteria dispersed from biofilms) on blood agar plates with treatments of CLR (4.8 µg/mL), CLR + AMX (9.6 µg/mL) and RHL/Cl-Ch-cal (with 4.8 µg/mL CLR). (D) MIC of free CLR and RHL/Cl-Ch-cal ($n = 6$). (E) Time curves of inhibition of bacterial adhesion ($n = 6$) by CLR (0.024 µg/mL, MIC), CLR + AMX (0.048 µg/mL) and RHL/Cl-Ch-cal (with 0.024 µg/mL CLR).

culture medium) and BHI (*H. pylori* culture medium) to test. In DMEM and BHI, RHL/Cl-Ch-cal nearly showed no change in particle size within 24 h (Fig. 1C and D). Moreover, RHL/Cl-Ch-cal remained relatively stable after a series of dilutions (Supporting Information Fig. S1). When the dilution ratio was relatively high, the diameter of RHL/Cl-Ch-cal increased slightly but still remained smaller than 200 nm, which was beneficial for

mucus penetration. Besides, RHL/Cl-Ch-cal could be stable at 4 °C for at least 28 days (Fig. 1E).

RHL/Cl-Ch-cal was -13.4 ± 0.2 mV in zeta potential (Fig. 1F), that was inclined to penetrate the negatively charged mucin-rich mucus layer[23] and reach *H. pylori* infection sites. In contrast, CS coated RHL/Cl-Ch-cal (CS/RHL/Cl-Ch-cal) was prepared as control group with positive zeta potential

(33.5 ± 1.0 mV) which was reported to have strong interaction with mucin. As expected, negatively charged RHL/Cl-Ch-cal had significantly lower mucin aggregation rate and stronger apparent permeability than positively charged CS/RHL/Cl-Ch-cal, displaying superior mucus penetration efficiency (Fig. 1G). However, RHL/Cl-Ch-cal would stay in stomachs before penetrating through the gastric mucus layer. Therefore, as little drug leakage as possible in the acidic environment would facilitate RHL/Cl-Ch-cal to carry more drugs through the mucus layer to reach *H. pylori* infection sites. In acidic environment, RHL/Cl-Ch-cal had a rapid release in the early stage, followed by a plateau phase, with a total leakage rate of about 20% within 6 h (Fig. 1H). In other words, RHL/Cl-Ch-cal could carry most of the drugs to *H. pylori* infection sites when it penetrated quickly through the gastric mucus layer.

H. pylori colonizes under the gastric mucus layer, where pH is close to neutral. However, bacteria usually produce a weak acid microenvironment around their infection sites[24]. To study the drug release behavior around *H. pylori* infection sites, the curves of cumulative release of RHL/Cl-Ch-cal at pH 5.5 were plotted (Fig. 1I and J). The curves of free CLR and calcitriol showed that free drugs were released rapidly, and both their cumulative release rates exceeded 90% in 2 h. By contrast, RHL/Cl-Ch-cal also had a rapid release in the first 2 h, followed by the slow release, and the cumulative release rate of CLR and calcitriol reached 60% and 70% at 24 h. In fact, this kind of rapid release at the beginning was beneficial to kill and eliminate bacteria.

Owing to *H. pylori* colonizing in stomachs, it would be more advantageous for treatments that more drugs staying in the stomachs rather than being absorbed into blood directly. As expected, longer duration of RHL/DiR-Ch-cal in mice stomach (Supporting Information Fig. S2A) might attribute to its effective penetration through gastric mucus layer, which was in favor of the arrival of drugs to infection sites and not easily to be removed. The pharmacokinetics study of CLR also confirmed that RHL/Cl-Ch-cal tended to be detained and released in the stomachs

(Supporting Information Fig. S2B). CLR reached its maximum concentration (9.7 ng/mL) in plasma at 2 h after oral administration of RHL/Cl-Ch-cal, which was lower and later than that after oral administration of free CLR (19.7 ng/mL at 1 h). Taken together, a series of characterization results showed that RHL/Cl-Ch-cal had good premises and key properties against *H. pylori* infection.

3.2. *H. pylori* biofilms eradication

During chronic infections, *H. pylori* easily forms biofilms that are much more resistant to antibiotics than the planktonic one[25]. CV staining (Fig. 2A) showed that CLR + RHL could obviously eradicate biofilms. Especially when these two were co-delivered in RHL/Cl-Ch-cal, the eradication rate to *H. pylori* biofilms was up to 88.11%. However, antibiotics combinations like CLR + AMX (one of clinical therapies) did not significantly improve biofilms eradication rate. The residual biofilms were further observed by SEM (Fig. 2B). *H. pylori* in BHI group (control) adhered tightly and formed biofilms, which widely distributed with classical aggregation. After treatment with free CLR and CLR + AMX, *H. pylori* membranes remained whole. In RHL/Cl-Ch-cal group, only sporadic bacteria attached and their surfaces were rough, and some of which were crimped and sunken with obvious fusion. We presumed that RHL/Cl-Ch-cal had membrane destruction effect on *H. pylori*, which would be favorable for *H. pylori* eradication without concern about resistance development.

Biofilms are composed of interior bacteria and protective barrier EPS, where two main EPS components proteins and polysaccharides play an important role in maintaining biofilm structure[26]. BCA protein assay kit and phenol-sulfuric acid measurement showed that RHL/Cl-Ch-cal significantly removed proteins and polysaccharides of EPS in *H. pylori* biofilms, possessing a higher removal rate of polysaccharides than that of proteins (Fig. 2C). It seemed to be related to the binding between RHL and metal ions[27], which destroyed the connection between metal ions
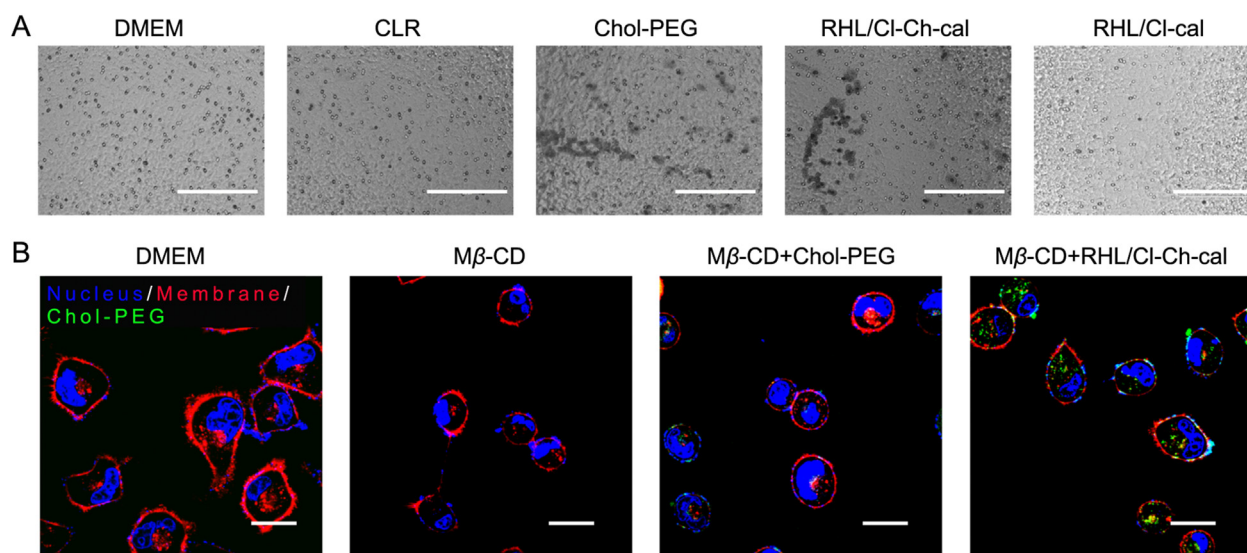

Figure 4 Macrophage migration and Chol-PEG transfer. (A) Macrophage migration detected by Transwell method after treatments of CLR (4.8 μg/mL), Chol-PEG (with 100 μg/mL Chol), RHL/Cl-Ch-cal (with 100 μg/mL Chol) and RHL/Cl-cal (without Chol-PEG). Scale bar = 200 μm. (B) Mβ-CD (5 mg/mL, 30 min) was used to deplete Chol in cell membrane. Chol-PEG transfer was observed under CLSM after incubation with Chol-PEG (green, FITC-labeled) and RHL/Cl-Ch-cal. Cell nuclei were stained as blue (DAPI) and cell membranes were red (DiD). Scale bar = 20 μm.

and polysaccharides in the biofilms network. Similar results were obtained under CLSM using fluorescence labeling (Supporting Information Fig. S3), where proteins were labeled by FITC and polysaccharides by ConA-FITC. After treatment with RHL/Cl-Ch-cal, polysaccharides and proteins in biofilms sparsely exited, suggesting that EPS were scattered and eradicated.

Although CLR eradicated *H. pylori* biofilms in a concentration dependent manner, the eradication rate raised slowly along with the concentration (Fig. 3A). Even when the concentration reached $1000 \times$ MIC (24 µg/mL), CLR did not completely remove biofilms, nor did kill interior *H. pylori*. It indicated that *H. pylori* biofilms did exhibit much stronger resistance to CLR than planktonic ones. In contrast, merely sparse green fluorescence and no red fluorescence in RHL/Ch-cal group manifested effective eradication of biofilms but poor killing of interior *H. pylori* due to the absence of antibacterial agents (Fig. 3B). Based on this, after treatment of RHL/Cl-Ch-cal with anti-*H. pylori* agent CLR loaded, red fluorescence was displayed, indicating its ability to kill *H. pylori* inside biofilms. This might be because the destruction of EPS made biofilms disperse to small granules where CLR was

easier to permeate to contact with interior *H. pylori*. When RHL/Cl-Ch-cal contained 4.8 µg/mL CLR, remained *H. pylori* was labeled with red fluorescence (Fig. 3B), demonstrating that almost all interior *H. pylori* was killed, where the content of CLR used was much lower than that of free CLR to achieve the same antibacterial effect.

H. pylori dispersed from biofilms was hard to be killed completely and timely, which could adhere again, forming new biofilms and even causing a new round of infection[28]. To explore the viability of dispersed *H. pylori*, the biofilms supernatants were cultured on blood agar plates (Fig. 3C). Expectedly, BHI group (untreated) showed a mass of live *H. pylori*. By contrast, no colony was observed in RHL/Cl-Ch-cal group, implying its strong killing ability on all forms of *H. pylori* including the planktonic one (Fig. 3D), the dispersed one from biofilms (Fig. 3C) and that in biofilms (Fig. 3B). However, it was almost impossible to kill all *H. pylori* in vivo, so inhibiting the residual one from adhering again was as important as both eradicating biofilms and killing *H. pylori*. Obviously, inhibiting the residual bacteria from adhering was the key step to cut biofilms re-fabrication[29]. As shown, not
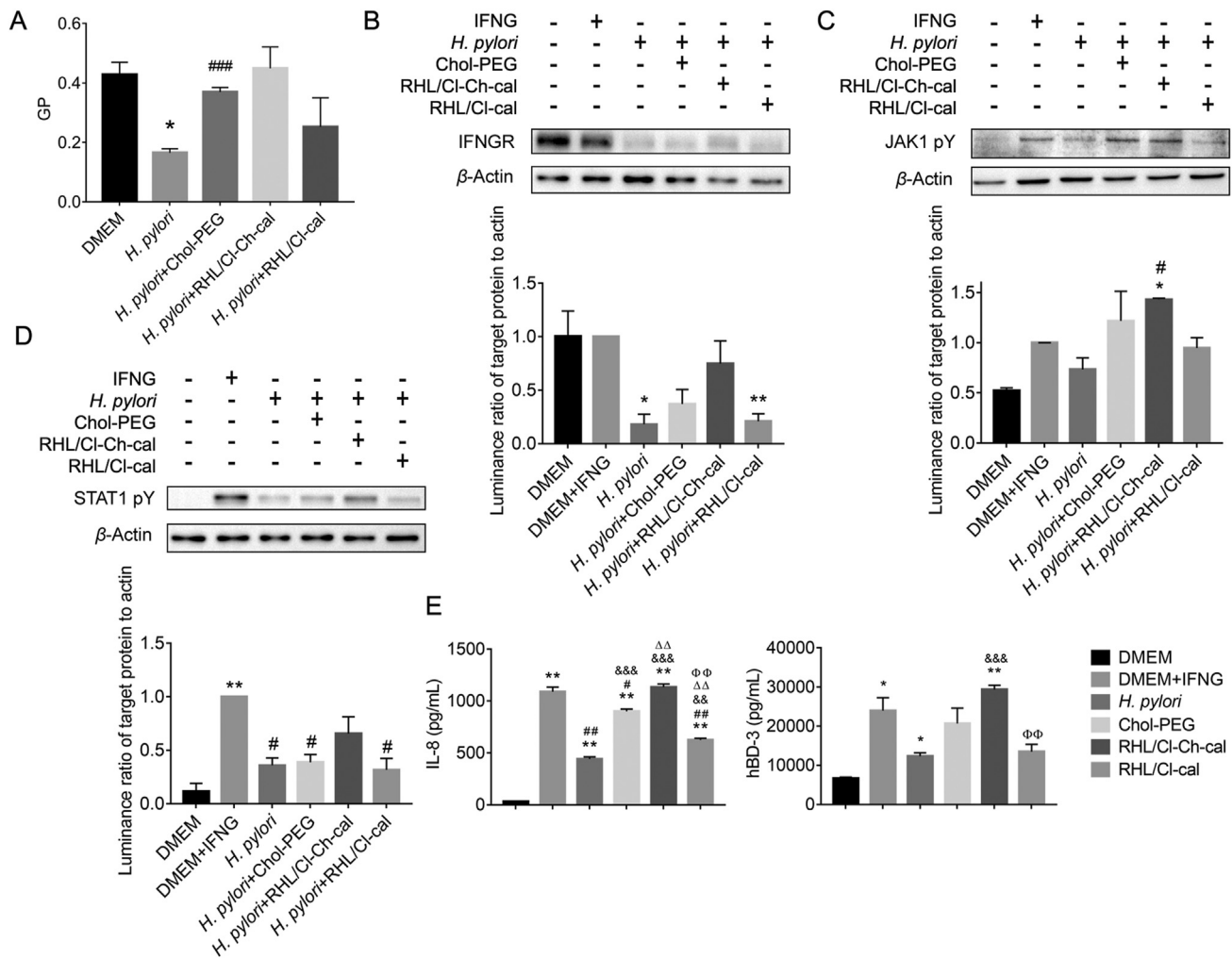

Figure 5 Activation of the downstream immune pathways. (A) Generalized polarization (GP) characterizing cell membrane fluidity was calculated ($n = 3$). *$P < 0.05$ *vs.* DMEM. ###$P < 0.001$ *vs.* *H. pylori*. Protein expressions of (B) IFNGR, (C) JAK1 phosphorylation and (D) STAT1 phosphorylation were detected by WB ($n = 3$). *$P < 0.05$ and **$P < 0.01$ *vs.* DMEM, #$P < 0.05$ *vs.* DMEM + IFNG (10 ng/mL, 30 min). (E) The secretions of IL-8 and hBD-3 were detected by ELISA ($n = 3$). *$P < 0.05$ and **$P < 0.01$ *vs.* DMEM, #$P < 0.05$ and ##$P < 0.01$ *vs.* DMEM + IFNG, &&$P < 0.01$ and &&&$P < 0.001$ *vs.* *H. pylori*, ΔΔ$P < 0.01$ *vs.* Chol-PEG, ΦΦ$P < 0.01$ *vs.* RHL/Cl-Ch-cal.

only the initial adhesion (2−4 h) of *H. pylori* was effectively inhibited by RHL/Cl-Ch-cal, even the amount of biofilm biomass never increased over the whole test time of 48 h (Fig. 3E).

3.3.   Host immune response activation

Complex microenvironment *in vivo* made *H. pylori* hard to be completely killed by antibiotics, and the residual ones would become a hidden danger ultimately causing treatment failure[30]. Host immune system was extremely crucial to help eliminate these residual pathogens. However, *H. pylori* could subtly achieve immune escape *via* depleting Chol in host cell membrane[14]. MGC803 cells were inoculated in acceptor Transwell wells beforehand, and then macrophages were added to donor chambers after *H. pylori* infection, simulating the immune cells migration to the infection sites *in vivo*. No macrophage migration was observed at 24 h after *H. pylori* infection, supporting the existence of immune escape (Fig. 4A). Free Chol-PEG and RHL/Cl-Ch-cal (Chol-PEG loaded) did increase macrophage migration, while antibiotics CLR and RHL/Cl-cal (without Chol-PEG) could not, indicating that exogenous Chol-PEG was able to activate host immune response. Meanwhile, this activation ability did not exist in some Chol analogues (Supporting Information Fig. S4). Methyl-*β*-cyclodextrin (M*β*-CD) depleted Chol in host cell membrane to simulate the pathological characteristics of *H. pylori* infection, which changed the cell morphology (Fig. 4B). FITC-labeled Chol-PEG was loaded into RHL/Cl-Ch-cal, which

coincided with the cell membrane in CLSM observation, suggesting that exogenous Chol-PEG could be inserted into cell membrane and do repair, although the cell morphology was still not well as the normal cells. The structure of RHL/Cl-Ch-cal was closer to cell membrane, thus the transfer of Chol-PEG between RHL/Cl-Ch-cal and cells was stronger.

The change of cell membrane fluidity would lead to the blue shift of membrane permeability fluorescence probe laurdan emission spectrum[31], so that the ratio of fluorescence intensity at different wavelengths, known as generalized polarization (GP), could characterize the cell membrane fluidity[32]. The significantly decreased GP value of cell membrane represented its notably decreased fluidity (Fig. 5A), which proved that *H. pylori* indeed depleted Chol in host cell membrane during prolonged infections. Free Chol-PEG and RHL/Cl-Ch-cal restored the cell membrane fluidity, indicating that the insertion of exogenous Chol-PEG was conducive to the reconstruction of lipid raft (a Chol-rich microdomain), and the cell membrane fluidity after RHL/Cl-Ch-cal treatment was not significantly different from that of normal cells.

Depletion of Chol damaging lipid raft, where IFNGR located, resulted in the degradation of IFNGR structure (Fig. 5B). IFNGR expression was partly restored after RHL/Cl-Ch-cal treatment, suggesting that its structure was remodeled, which facilitated gastric epithelial cells to receive signals to trigger downstream immune responses. Lipid raft-dependent receptors (*e.g.*, IFNGR) would stimulate immune responses to defend against mucosal pathogens by activating Janus kinase/signal transducer and
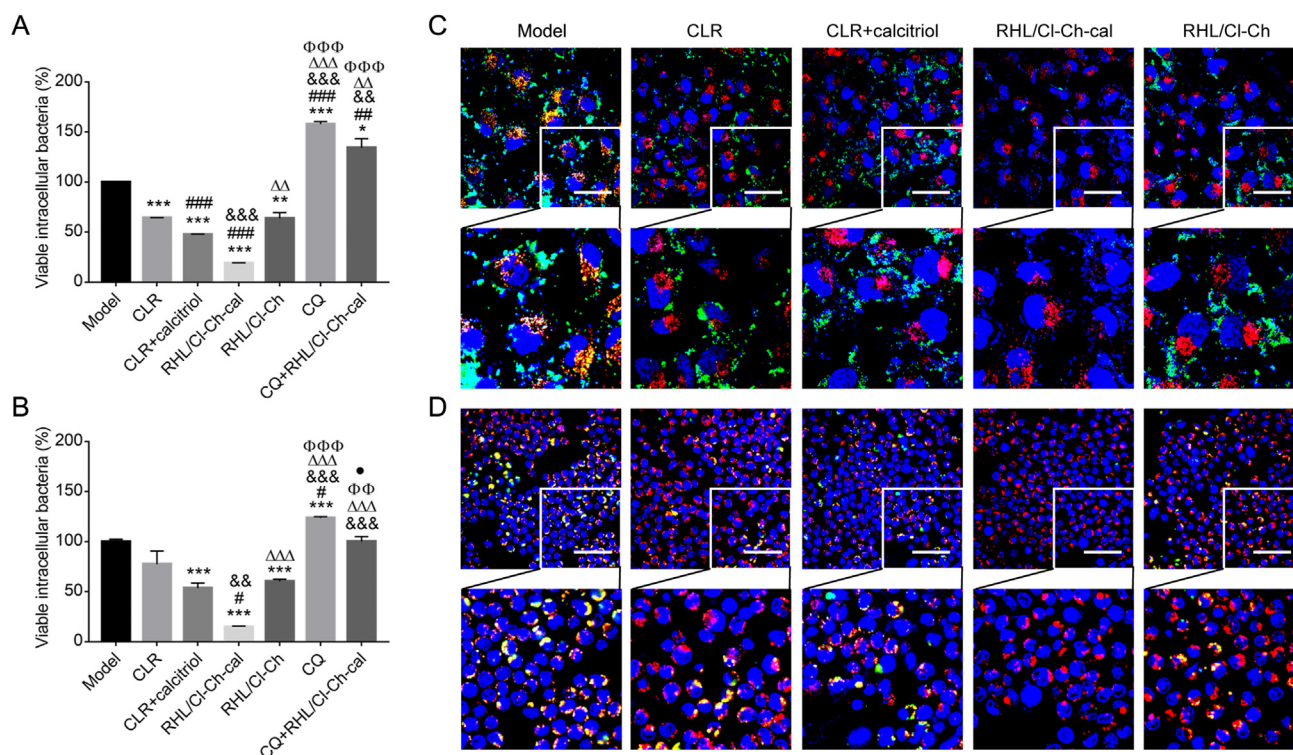

Figure 6   Killing of intracellular *H. pylori*. The percentages of viable intracellular *H. pylori* in (A) MGC803 cells and (B) RAW264.7 cells ($n = 4$). Here, CLR (0.024 μg/mL), CLR + calcitriol (0.1 μg/mL), RHL/Cl-Ch-cal (with calcitriol) and RHL/Cl-Ch (without calcitriol) were incubated with cells. CQ (20 μmol/L) was co-incubated with drugs as a lysosomal inhibitor. *$P < 0.05$, **$P < 0.01$ and ***$P < 0.001$ *vs.* Model, #$P < 0.05$, ##$P < 0.01$ and ###$P < 0.001$ *vs.* CLR, &&$P < 0.01$ and &&&$P < 0.001$ *vs.* CLR + calcitriol, ΔΔ$P < 0.01$ and ΔΔΔ$P < 0.001$ *vs.* RHL/Cl-Ch-cal, ΦΦ$P < 0.01$ and ΦΦΦ$P < 0.001$ *vs.* RHL/Cl-Ch, •$P < 0.01$ *vs.* CQ. CLSM images of intracellular *H. pylori* in (C) MGC803 cells and (D) RAW264.7 cells were presented. Intracellular *H. pylori* were green (CFDA-SE), cell nuclei were blue (DAPI) and lysosomes were red (DND-99). Scale bar = 50 μm.

activator of transcription (JAK/STAT) pathway[33]. WB results showed that *H. pylori* infections had little effect on JAK1 (Fig. 5C), but significantly reduced STAT1 phosphorylation signals (Fig. 5D). Therefore, prolonged *H. pylori* infection first destroyed lipid raft and degraded IFNGR, and then blocked phosphorylation of JAK/STAT, thereby suppressing downstream immune responses. Herein, JAK1 and STAT1 signals were enhanced after RHL/Cl-Ch-cal remodeling the structure of IFNGR (Fig. 5B−D). Furthermore, the expression of chemokines interleukin-8 (IL-8, a chemokine for neutrophils) and human β-defensin 3 (hBD3, a natural host antimicrobial peptide) were also restored (Fig. 5E), which had been blocked by *H. pylori* infection[34,35]. The expression of IL-8 after RHL/Cl-Ch-cal treatment was not significantly different from that of normal cell under stress (IFNG-treated), indicating that the recovery of IL-8 would not aggravate the host inflammatory response. Besides, the significant decrease in hBD3 expression led by the blocking of upstream immune pathways, was enhanced after RHL/Cl-Ch-cal treatment, and its level was higher than that of normal cell under stress. Overall, RHL/Cl-Ch-cal treatment was beneficial to enhance the host clearance of pathogen *H. pylori* by restoring the normal immune response.

3.4. Intracellular *H. pylori* killing activity

The bacterium death was not the sole destiny of macrophage phagocytosis, on the contrary, *H. pylori* could survive in the damaged lysosomes of macrophages and even in those of gastric epithelial cells[17,18]. Therefore, killing intracellular bacteria became another key point to defend persistent infections. Intracellular *H. pylori* model *in vitro* was successfully established with

cell survival rates more than 90% (Supporting Information Fig. S5). By plate counting method, the survival rates of intracellular *H. pylori* decreased prominently to 19.0% (MGC803 cells) and 14.8% (RAW264.7 cells) after RHL/Cl-Ch-cal treatment, respectively (Fig. 6A and B). Importantly, the killing effect of RHL/Cl-Ch-cal on intracellular *H. pylori* was strongly counteracted by the lysosomal inhibitor CQ, which could increase the pH value of lysosomes by neutralizing H^+ to inhibit the activity of hydrolases.

Next, the clearance effect of intracellular bacteria was examined by CLSM (Fig. 6C and D), and the results were in well accordance with the plate counting results. *H. pylori* in model group co-localized well with lysosomes in both MGC803 cells and RAW264.7 cells, indicating that the niche for intracellular *H. pylori* to survive was indeed lysosome. The difference was that, after drug treatment, numerous intracellular *H. pylori* distributed to extracellular space of MGC803 cells (Fig. 6C) while most *H. pylori* still located in lysosomes of RAW264.7 cells (Fig. 6D). We hypothesized that *H. pylori* could temporarily survive in gastric epithelial cells (*e.g.*, MGC803 cells) to escape from the adverse environment, once drugs withdrew or environment got better, the intracellular *H. pylori* would flee away and distribute to somewhere else to trigger new infections. In contrast, *H. pylori* was difficult to flee from lysosomes of macrophages due to the macrophage phagocytosis, therefore having a good co-localization with lysosomes of RAW264.7 cells.

Ideally, in lysosomes H^+ was absorbed while Ca^{2+} was excreted by MCOLN3 to maintain charge balance, which was critical to the acidification maturity of lysosomes and the latter was responsible for bacteria degradation. However, when *H. pylori* survived in impaired lysosomes[36], the expression of
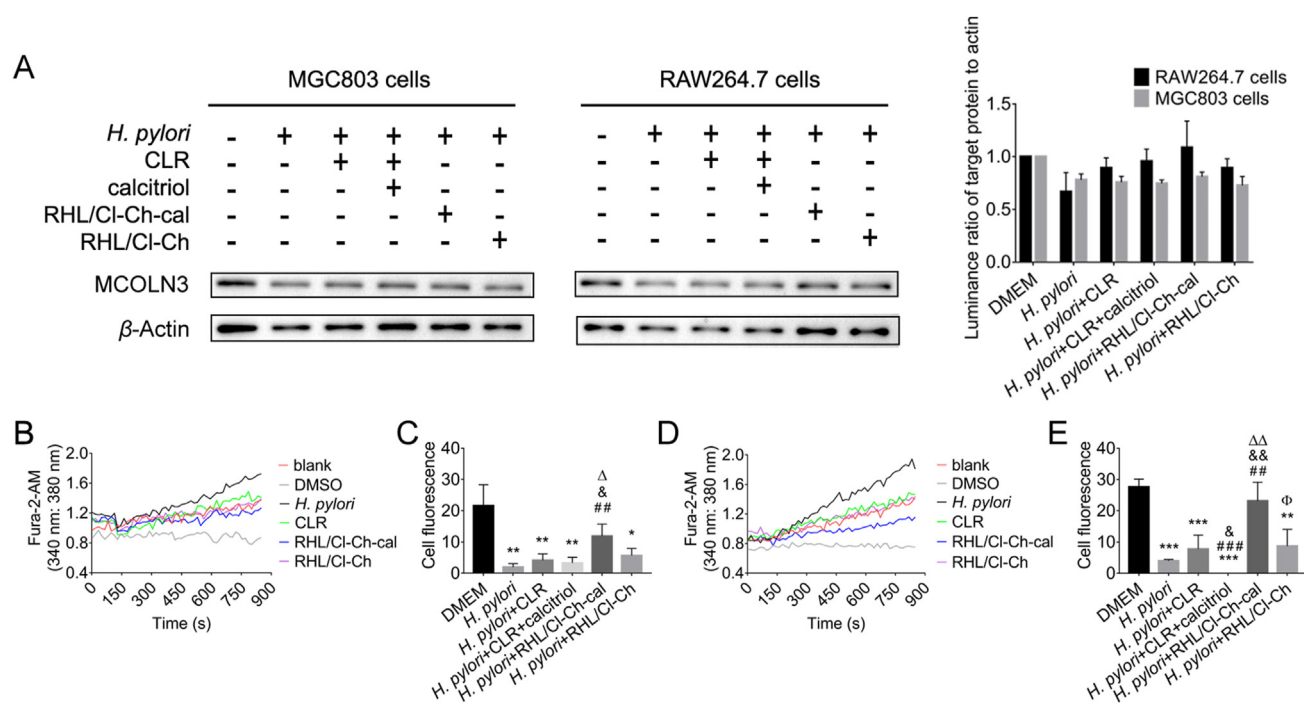

Figure 7 Characterizations of lysosomal functions. (A) Protein expressions of MCOLN3 detected by WB. Detection of Ca^{2+} levels in (B) MGC803 cells and (D) RAW264.7 cells. Degrees of lysosomal acidification in (C) MGC803 cells and (E) RAW264.7 cells. *$P < 0.05$, **$P < 0.01$ and ***$P < 0.001$ *vs.* DMEM. ##$P < 0.01$ and ###$P < 0.001$ *vs.* *H. pylori*. &$P < 0.05$ and &&$P < 0.01$ *vs.* *H. pylori* + CLR. ∆$P < 0.05$ and ∆∆$P < 0.01$ *vs.* *H. pylori* + CLR + calcitriol. Φ$P < 0.05$ *vs.* *H. pylori* + RHL/Cl-Ch-cal. Data are presented as mean ± SD (n = 3).

MCOLN3 was decreased (Fig. 7A). That was, Ca^{2+} might not be discharged, resulting in Ca^{2+} overaccumulation in lysosomes (Fig. 7B and D), and then H$^+$ could not be absorbed as usual. Eventually, abnormal lysosomal acidification happened (Fig. 7C and E). CLR and CLR + calcitriol played a poor role in the recovery of lysosomal acidification in *H. pylori*-infected cells. Comparatively, after RHL/Cl-Ch-cal treatment, MCOLN3 expression increased and excessive Ca^{2+} outflow was induced to impel lysosomal acidification, which was very close to that of normal cells (Fig. 7). Compared with RAW264.7 cells, the effect of drugs on MGC803 cells was weaker, indicating again that epithelial cells were temporary shelter for *H. pylori* to escape from

adverse environment, where its intracellular and extracellular distribution might be a dynamic equilibrium.

3.5. *In vivo* anti-*H. pylori* efficacy

Then *in vivo* efficacy and tissue toxicity in *H. pylori*-infected C57Bl/6 mice were further tested, where 1×10^8 CFU of *H. pylori* SS1 was orally administered for 7 times on Days 1, 3, 5, 7, 9, 11 and 13 respectively (Fig. 8A). About two weeks after inoculation, five blank mice and five model mice were randomly selected and sacrificed. The positive results (purple) of rapid urease assay (Fig. 8B) and the Cp values of QPCR (Supporting Information
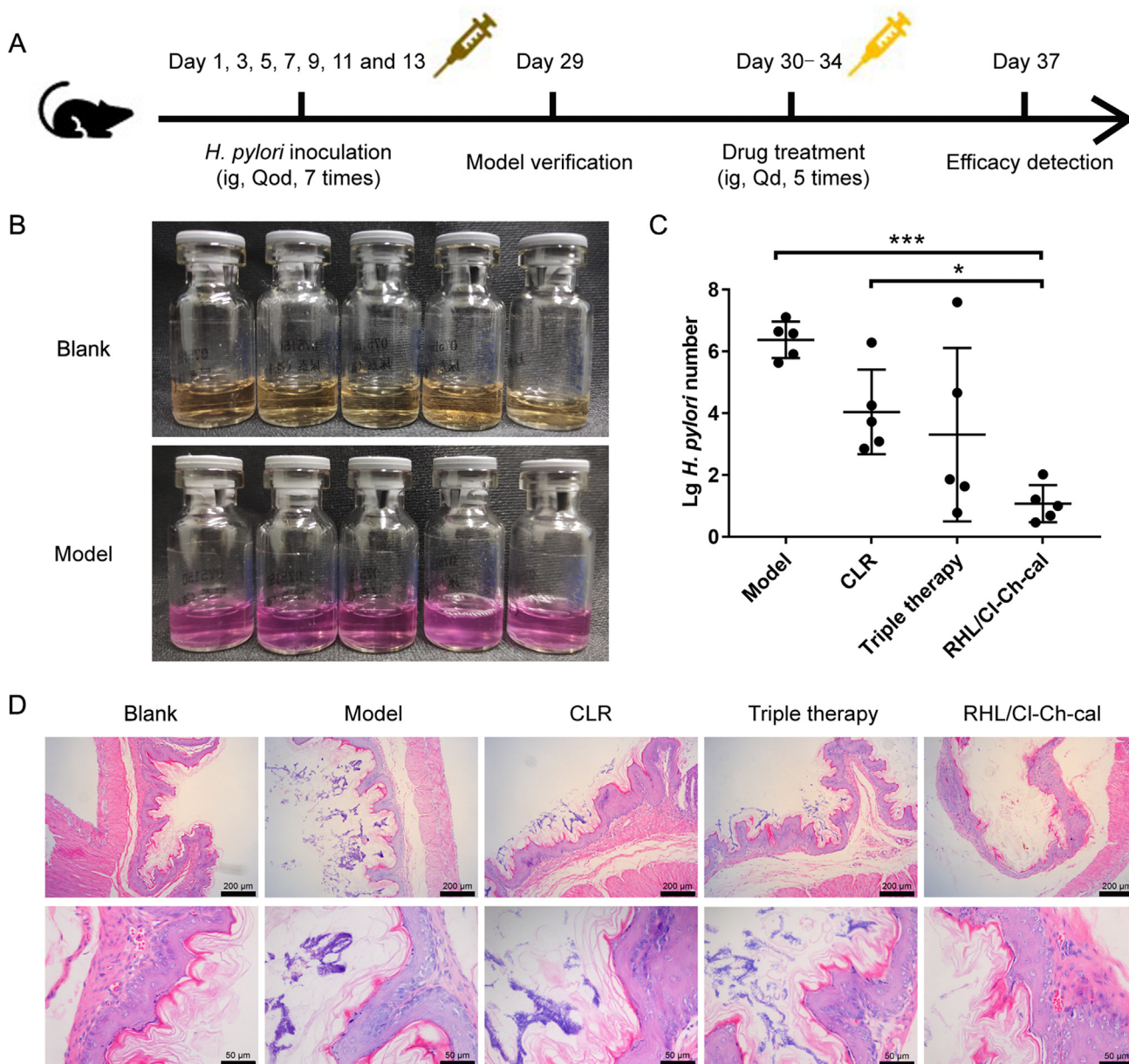

Figure 8 *In vivo H. pylori*-infected mice models and antibacterial efficacy of RHL/Cl-Ch-cal. (A) Workflow for mice model construction and drug treatment. (B) Model verification by rapid urease assay. (C) *H. pylori* burdens in mice stomachs after treatments with CLR (64 μg/kg), triple therapy [CLR + AMX (128 μg/kg) + lansoprazole (3.84 μg/kg)] and RHL/Cl-Ch-cal (with 64 μg/kg CLR) once per day continuedly for 5 days. Data were mean ± SD ($n = 5$), *$P < 0.05$ and ***$P < 0.001$. (D) Histopathology of mice stomachs by H&E staining. Scale bar = 200 μm in upper row, scale bar = 50 μm in nether row.

Fig. S6) indicated that the *in vivo H. pylori* models were successfully established. *H. pylori*-infected mice were divided into four groups ($n = 5$, for each group) and orally administered with PBS, free CLR, free CLR + AMX + lansoprazole (clinical triple therapy) and RHL/Cl-Ch-cal once a day for 5 consecutive days. The *in vivo* efficacies were evaluated *via* calculating the *H. pylori* burdens in mice stomach by QPCR (Fig. 8C). The mean gastric *H. pylori* burdens of free CLR and triple therapy were $10^{4.05}$ CFU and $10^{3.31}$ CFU respectively, which showed no statistical difference compared with $10^{6.38}$ CFU of *H. pylori* burden in model group. Among them, even though the mean *H. pylori* burden was reduced by 3 orders of magnitude after triple therapy treatment, there was an obvious difference within the group, suggesting that some mice formed refractory infections in stomachs and escaped the attack of free antibiotics. After oral administration of RHL/Cl-Ch-cal, the mean *H. pylori* burden was significantly reduced to $10^{1.08}$ CFU, which was statistically different from both model group and CLR group, and the difference within the group was small, suggesting that RHL/Cl-Ch-cal had a remarkable anti-*H. pylori* effect *in vivo*.

Meanwhile, H&E staining was performed to evaluate the toxicity and the efficacy of RHL/Cl-Ch-cal in mice (Fig. 8D). In blank group (without *H. pylori* infection), the parietal cells, chief cells and mucous neck cells were clearly visible, and there was no tissue edema or inflammatory cells infiltration and no *H. pylori* aggregation in the keratinized layer. In model group, numerous *H. pylori* were observed diffusely colonizing on the surface of gastric mucosa, around 20%−30% of the whole area. This kind of the thick communities of bacteria under microscope observation could be considered as the formation of typical biofilms *in vivo*. After free CLR treatment, inflammatory cell infiltration was in the local laminae propria, and *H. pylori* (10%−20%) still existed. After triple therapy, a small amount of *H. pylori* (5%−10%) were in the keratinized layer, in which the *in vivo* effect was superior to free CLR. Comparatively, only a few *H. pylori* (1%−5%) remained and there was no tissue edema or inflammatory cell infiltration in RHL/Cl-Ch-cal group, indicating that RHL/Cl-Ch-cal were safe in mice.

4. Conclusions

H. pylori eradication rate inevitably decreases along with antibiotics resistance raising, especially when biofilms form followed by chronic infections, which intensively challenges the anti-*H. pylori* therapies due to frequent refractory infections[37,38]. In addition, by depleting Chol of lipid raft on the gastric epithelial cell membrane, *H. pylori* damages the related cytokine receptor structures and hence blocks the downstream immune pathways and macrophage phagocytosis[14]. *H. pylori* even escapes from adverse circumstances through intracellular survival in macrophages and gastric epithelial cells[17]. Hence, biofilm formation, immune escape and intracellular survival contribute to *H. pylori* refractory infections together.

Based on our previous researches regarding refractory biofilms (biofilms eradication tetralogy)[11,12] and consideration for immune escape and intracellular survival of *H. pylori*, herein multifunctional RHL/Cl-Ch-cal was designed to improve *H. pylori* clearance rate and therefore reduce recurrence rate. In summary, RHL/Cl-Ch-cal first penetrated through mucus layer to the infection sites where RHL shell destroyed *H. pylori* biofilms making interior bacteria be exposed to CLR. RHL/Cl-Ch-cal inhibited the re-adhesion of residual bacteria to block biofilms regeneration. Then, exogenous Chol provided by RHL/Cl-Ch-cal restored the lipid raft

on host cell membrane damaged by *H. pylori*, and therewith activated the downstream JAK/STAT immune pathways. Subsequently, macrophage phagocytose was induced to clear the remained planktonic *H. pylori*, and antimicrobial peptide hBD3 was secreted to kill *H. pylori*. Finally, the combination of calcitriol and CLR restored the expression of MCOLN3 to recover the normal exchange of H^+ and Ca^{2+} in lysosomes and achieve lysosomal acidification, which played a critical role on intracellular *H. pylori* degradation.

According to the Kyoto Global Consensus report, *H. pylori* infection is a disease state that should be eradicated unless there are countervailing factors[39]. Therefore, improving *H. pylori* clearance rate is of great significance to treat *H. pylori* infection. In addition, using nanotechnology to deliver antibacterial drugs would improve their antibacterial efficiencies[40]. Based on the proposed combined contributions of biofilms formation, immune escape and intracellular survival to *H. pylori* refractory infections, RHL/Cl-Ch-cal was designed as a "comprehensive attack" strategy to improve the *H. pylori* clearance rate through biofilms eradication tetralogy, immune activation and intracellular bacteria killing to achieve the purpose of eradicating *H. pylori* in the complex environment.

Author contributions

Xiaonan Chen conceived the idea, carried out the experiments and performed data analysis. Yiqing Zou, Shuqi Zhang, Pengchao Fang, Shuxuan Li, Pengyu Li and Yingying Sun participated part of the experiments. Gang Yuan advised on the research. Haiyan Hu supervised the idea and the experiments. The manuscript was written by Xiaonan Chen and Haiyan Hu. All authors contributed to the general discussion and reviewed the manuscript.

Conflicts of interest

The authors have no conflicts of interest to declare.

Appendix A. Supporting information

Supporting data to this article can be found online at https://doi.org/10.1016/j.apsb.2022.05.014.

References

1. Hooi JKY, Lai WY, Ng WK, Suen MMY, Underwood FE, Tanyingoh D, et al. Global prevalence of *Helicobacter pylori* infection: systematic review and meta-analysis. *Gastroenterology* 2017; **153**:420−9.
2. Mladenova I. Clinical relevance of *Helicobacter pylori* infection. *J Clin Med* 2021;**10**:3473.
3. Backert S, Neddermann M, Maubach G, Naumann M. Pathogenesis of *Helicobacter pylori* infection. *Helicobacter* 2016;**21**:19−25.
4. Duan FJ, Song CH, Shi JC, Wang P, Ye H, Dai LP, et al. Identification and epidemiological evaluation of gastric cancer risk factors: based on

a field synopsis and meta-analysis in Chinese population. *Aging-US* 2021;**13**:21451−69.

5. Oster P, Vaillant L, Riva E, McMillan B, Begka C, Truntzer C, et al. *Helicobacter pylori* infection has a detrimental impact on the efficacy of cancer immunotherapies. *Gut* 2022;**71**:457−66.

6. Gupta P, Sarkar S, Das B, Bhattacharjee S, Tribedi P. Biofilm, pathogenesis and prevention−a journey to break the wall: a review. *Arch Microbiol* 2016;**198**:1−15.

7. Cammarota G, Branca G, Ardito F, Sanguinetti M, Ianiro G, Cianci R, et al. Biofilm demolition and antibiotic treatment to eradicate resistant *Helicobacter pylori*: a clinical trial. *Clin Gastroenterol Hepatol* 2010;**8**:817−20.

8. Coticchia JM, Sugawa C, Tran VR, Gurrola J, Kowalski E, Carron MA. Presence and density of *Helicobacter pylori* biofilms in human gastric mucosa in patients with peptic ulcer disease. *J Gastrointest Surg* 2006;**10**:883−9.

9. Yonezawa H, Osaki T, Hanawa T, Kurata S, Ochiai K, Kamiya S. Impact of *Helicobacter pylori* biofilm formation on clarithromycin susceptibility and generation of resistance mutations. *PLoS One* 2013;**8**:e73301.

10. Flemming HC, Wingender J. The biofilm matrix. *Nat Rev Microbiol* 2010;**8**:623−33.

11. Li PY, Chen XN, Shen YN, Li HT, Zou YQ, Yuan G, et al. Mucus penetration enhanced lipid polymer nanoparticles improve the eradication rate of *Helicobacter pylori* biofilm. *J Control Release* 2019;**300**:52−63.

12. Shen YN, Zou YQ, Chen XN, Li PY, Rao YQ, Yang X, et al. Antibacterial self-assembled nanodrugs composed of berberine derivatives and rhamnolipids against *Helicobacter pylori*. *J Control Release* 2020;**328**:575−86.

13. Xu Z, Li BQ, Du YQ, Zhang RQ, Tong XH, Li J, et al. *Helicobacter pylori* regulates ILK to influence autophagy through Rac 1 and RhoA signaling pathways in gastric epithelial cells. *Microb Pathog* 2021;**158**:105054.

14. Wunder C, Churin Y, Winau F, Warnecke D, Vieth M, Lindner B, et al. Cholesterol glucosylation promotes immune evasion by *Helicobacter pylori*. *Nat Med* 2006;**12**:1030−8.

15. Blouin CM, Hamon Y, Gonnord P, Boularan C, Kagan J, Lesegno CVD, et al. Glycosylation-dependent IFN-gammaR partitioning in lipid and actin nanodomains is critical for JAK activation. *Cell* 2016;**166**:920−34.

16. Bellavite P. Causality assessment of adverse events following immunization: the problem of multifactorial pathology. *F1000Res* 2020;**9**:170.

17. Dubois A, Boren T. *Helicobacter pylori* is invasive and it may be a facultative intracellular organism. *Cell Microbiol* 2007;**9**:1108−16.

18. Petersen AM, Krogfelt KA. *Helicobacter pylori*: an invading microorganism?. A review. *FEMS Immunol Med Microbiol* 2003;**36**:117−26.

19. Martina JA, Lelouvier B, Puertollano R. The calcium channel mucolipin-3 is a novel regulator of trafficking along the endosomal pathway. *Traffic* 2009;**10**:1143−56.

20. Hu W, Zhang L, Li MX, Shen J, Liu XD, Xiao ZG, et al. Vitamin D3 activates the autolysosomal degradation function against *Helicobacter pylori* through the PDIA3 receptor in gastric epithelial cells. *Autophagy* 2019;**15**:707−25.

21. Hardy DJ. Extent and spectrum of the antimicrobial activity of clarithromycin. *Pediatr Infect Dis J* 1993;**12**:S99−105.

22. Baraldi E, Lindahl O, Savic M, Findlay D, Ardal C. Antibiotic pipeline coordinators. *J Law Med Ethics* 2018;**46**:25−31.

23. Zhang YD, Li HB, Wang Q, Hao XY, Li HM, Sun HQ, et al. Rationally designed self-assembling nanoparticles to overcome mucus and epithelium transport barriers for oral vaccines against *Helicobacter pylori*. *Adv Funct Mater* 2018;**28**:1802675.

24. Radovic-Moreno AF, Lu TK, Puscasu VA, Yoon CJ, Langer R, Farokhzad OC. Surface charge-switching polymeric nanoparticles for bacterial cell wall-targeted delivery of antibiotics. *ACS Nano* 2012;**6**:4279−87.

25. Yonezawa H, Osaki T, Kamiya S. Biofilm formation by *Helicobacter pylori* and its involvement for antibiotic resistance. *BioMed Res Int* 2015;**2015**:914791.

26. Hobley L, Harkins C, MacPhee CE, Stanley-Wall NR. Giving structure to the biofilm matrix: an overview of individual strategies and emerging common themes. *FEMS Microbiol Rev* 2015;**39**:649−69.

27. Chen WF, Qu Y, Xu ZH, He FF, Chen Z, Huang SS, et al. Heavy metal (Cu, Cd, Pb, Cr) washing from river sediment using biosurfactant rhamnolipid. *Environ Sci Pollut Res Int* 2017;**24**:16344−50.

28. Rumbaugh KP, Sauer K. Biofilm dispersion. *Nat Rev Microbiol* 2020;**18**:571−86.

29. Roy R, Tiwari M, Donelli G, Tiwari V. Strategies for combating bacterial biofilms: a focus on anti-biofilm agents and their mechanisms of action. *Virulence* 2018;**9**:522−54.

30. Abadi ATB. Strategies used by *helicobacter pylori* to establish persistent infection. *World J Gastroenterol* 2017;**23**:2870−82.

31. Parasassi T, De Stasio G, d'Ubaldo A, Gratton E. Phase fluctuation in phospholipid membranes revealed by laurdan fluorescence. *Biophys J* 1990;**57**:1179−86.

32. Scheinpflug K, Krylova O, Strahl H. Measurement of cell membrane fluidity by laurdan GP: fluorescence spectroscopy and microscopy. *Methods Mol Biol* 2017;**1520**:159−74.

33. Choi JH, Cho SO, Kim H. Alpha-lipoic acid inhibits expression of IL-8 by suppressing activation of MAPK, Jak/Stat, and NF-kappaB in *H. pylori*-infected gastric epithelial AGS cells. *Yonsei Med J* 2016;**57**:260−4.

34. Bauer B, Wex T, Kuester D, Meyer T, Malfertheiner P. Differential expression of human beta defensin 2 and 3 in gastric mucosa of *Helicobacter pylori*-infected individuals. *Helicobacter* 2013;**18**:6−12.

35. Zhang HX, Zhang YX, Song ZF, Li RZ, Ruan H, Liu Q, et al. sncRNAs packaged by *Helicobacter pylori* outer membrane vesicles attenuate IL-8 secretion in human cells. *Int J Med Microbiol* 2020;**310**:151356.

36. Zhang L, Hu W, Cho CH, Chan FK, Yu J, Fitzgerald JR, et al. Reduced lysosomal clearance of autophagosomes promotes survival and colonization of *Helicobacter pylori*. *J Pathol* 2018;**244**:432−44.

37. McColl KE. Clinical practice. *Helicobacter pylori* infection. *N Engl J Med* 2010;**362**:1597−604.

38. Cammarota G, Sanguinetti M, Gallo A, Posteraro B. Review article: biofilm formation by *Helicobacter pylori* as a target for eradication of resistant infection. *Aliment Pharmacol Ther* 2012;**36**:222−30.

39. Sugano K, Tack J, Kuipers EJ, Graham DY, El-Omar EM, Miura S, et al. Kyoto global consensus report on *Helicobacter pylori* gastritis. *Gut* 2015;**64**:1353−67.

40. Tian XH, Wang PL, Li T, Huang XM, Guo WB, Yang YQ, et al. Selfassembled natural phytochemicals for synergistically antibacterial application from the enlightenment of traditional Chinese medicine combination. *Acta Pharm Sin B* 2020;**10**:1784−95.